IEEE Access
Multidisciplinary | Rapid Review | Open Access Journal

Received 25 October 2023, accepted 13 November 2023, date of publication 21 November 2023,
date of current version 29 November 2023.

Digital Object Identifier 10.1109/ACCESS.2023.3335811

RESEARCH ARTICLE

Nonlinear Analytical Model of Linear Switched Reluctance Motor With Segmented Secondary Considering Iron Saturation and End Effect

ZHIPENG LI[1], DAOHAN WANG[1], (Member, IEEE), CAN HUANG[2], SHUANG XU[1], AND XIUHE WANG[1], (Member, IEEE)

[1]School of Electrical Engineering, Shandong University, Jinan 250061, China
[2]Shandong Electric Power Engineering Consulting Institute Company Ltd., Jinan 250199, China

Corresponding author: Daohan Wang (dhwang@sdu.edu.cn)

This work was supported in part by the National Natural Science Foundation of China under Grant 51977125, and in part by the Shenzhen Fundamental Research Program under Grant JCYJ20220530141007017 and Grant JCYJ20210324141409023.

ABSTRACT Linear switched reluctance motor with segmented secondary (LSRMSS) is a new type of linear switched reluctance motor (LSRM) and has become an alternative for direct linear driving systems due to its high power and thrust density compared to the conventional LSRM. Performance estimation of LSRMSS is a tough task because of its critical local saturation effect on iron. To precisely estimate and investigate the dynamic performance of LSRMSS, a highly efficient and accurate nonlinear inductance function (NIF) considering iron saturation effects is developed in this paper. The inductance model of LSRMSS is derived based on an established magnetic equivalent circuit (MEC), facilitating machine performance estimation. The accuracy of the model is verified by comparing the results with finite element simulations (FEA). The end effect and mutual inductance effect are considered to improve the accuracy of the proposed NIF model, and key dimensions affecting machine performance are considered. Finally, the prototype of LSRMSS is manufactured, and the experimental testing platform is built. The measured results are in good agreement with the simulation results, validating the feasibility of the proposed nonlinear model.

INDEX TERMS Linear switched reluctance motor with segmented secondary (LSRMSS), nonlinear inductance function, the saturation effect, mutual inductance, end effects.

I. INTRODUCTION

Conventional transportation systems, especially long-distance transportation, are driven by rotary machines. It has many distinct shortcomings, such as a complex structure, low transportation efficiency, and a large friction force [1], [2]. In recent years, linear motor transportation systems have gradually become the main choice. Linear motor transportation systems are an excellent alternative to conventional rotary machine transportation systems. The driving of a linear motor transportation system only depends on the electromagnetic force between the primary mover and secondary stator. With the rapid development of servo control technology and power electronic devices, linear motor transportation systems have been widely applied in many industrial fields, such as urban rail transit, naval vessels, aircraft, the ejection device of unmanned aerial vehicles, high-rise construction elevators, and mine hoist systems [3], [4], [5], [6], [7].

Linear switched reluctance motor (LSRM) transportation system is an excellent alternative to conventional rotary machine transportation systems. It not only saves space but also reduces the total quality of the driving system. Thus, the thrust density and the payload ratio are improved [8], [9], [10], [11], [12]. The special structure characteristics of LSRM can be divided into several aspects, as follows:

1) The operating range of LSRM is wide, so it has good application potential in long-distance propulsion systems. Besides, the advantages of LSRM are obvious, such as its high reliability, low cost, and strong ability for frequent and continuous starting. LSRM can be controlled to operate

The associate editor coordinating the review of this manuscript and approving it for publication was Wencong Su.

within the optimal working range through various flexible control strategies.

2) LSRM has strong fault-tolerant ability. When single-phase winding or a power converter breaks down, the movement direction of the LSRM is constant. It has important practical significance for the driving systems of elevators and vertical elevators that require high running safety and reliability.

In recent years, LSRM has been widely used in long-distance transportation. It is becoming more and more important to estimate and research the dynamic performance of LSRM. The conventional LSRM has a low thrust density, and the secondary side cannot be modularized. Thus, with the development of the transportation field, the performance of conventional LSRM cannot meet the requirements of transportation systems.

In conventional LSRM, the adjacent teeth of the secondary stator connect with each other and are not segmented, which brings many difficulties to the installation of the secondary stator in long rail transit. Besides, in order to obtain sufficient thrust and a small force ripple, two phases or multiphases are required to work simultaneously in actual operation. A strange phenomenon occurs: the magnetic flux density of some parts is very high, and most of the other yokes have no magnetic flux. Therefore, the conventional LSRM has a lower utilization ratio of ferromagnetic material, resulting in a lower power and force density.

LSRMSS is a new type of LSRM, and its stator is composed of segmented secondary LSRMSS has some advantages in terms of simple structure, low manufacturing cost, higher power density, and higher thrust density compared with conventional LSRM [13], [14], [15]. LSRMSS has been an excellent alternative to conventional long-distance transportation systems. Performance estimation of LSRMSS is a tough task due to its critical local saturation effect of iron. Precise position control and a smooth force profile are always required in LSRM because of the requirements of low cruising velocity and variable load. In an actual linear actuator, the discrepancy between the generated force and the command force can be large due to the slow rise rate of the phase current. Our previous work presents a new control strategy based on the force distribution function for the LSRMSS [16]. In order to realize the control effect, it is necessary to estimate the inductance value of the motor in real time. This paper focuses on the construction of an efficient and accurate nonlinear inductance model that can be applied to the control of LSRMSS. Then the end effect and mutual inductance are considered to improve the nonlinear inductance model and make it more accurate.

The accurate estimation of inductance is an important issue in switched reluctance motors. Many papers have researched this question and put forward some methods such as 2-D table lookup, mathematical fitting, and neural network fitting [17], [18], [19], [20]. Finite element analysis (FEA) is a common method to calculate the values of inductance. However, this method requires a lot of numerical calculations and can be very time- consuming. Thus, the modular equivalent magnetic circuit (EMC) using mesh generations of LSRMSS is presented to estimate the inductance for special mover positions such as aligned positions and unaligned positions [21].

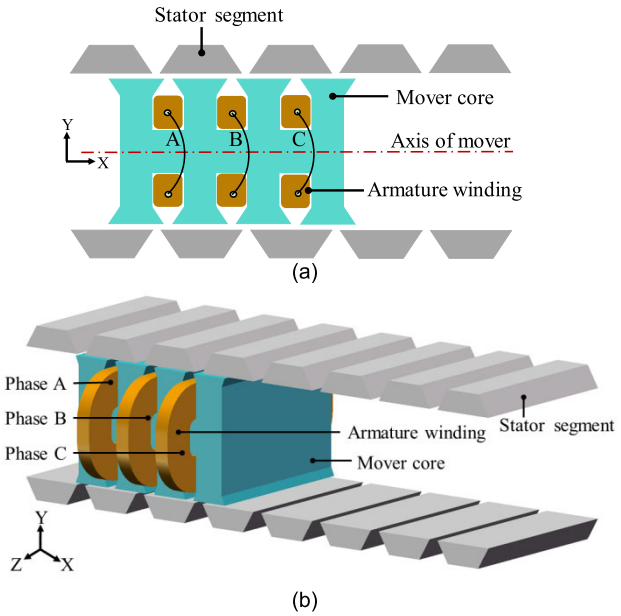

FIGURE 1. Three phase configuration of the LSRMSS. (a) 3D view of the LSRMSS. (b) Three phase configuration of the LSRMSS.

TABLE 1. Specific dimensions of LSRMSS.

Parameter	Value
Number of phases, m	3
Number of mover teeth, N_m	4
Air-gap length, l_g	0.5 mm
Stack length, L	60 mm
Number of turns per phase, N_{ph}	168
Interval width between segments, b_{ms}	2.67 mm
Mover tooth width, b_{mt}	18.75 mm
Mover tooth tip width, b_{os}	5.39 mm
Mover tooth tip height, h_{mt}	3.02mm
Mover yoke height, h_{my}	16.10 mm
Segment slope angle, θ_s	42°
Stator pole pitch, τ_s	32.12 mm
Mover pole pitch, τ_m	21.42 mm

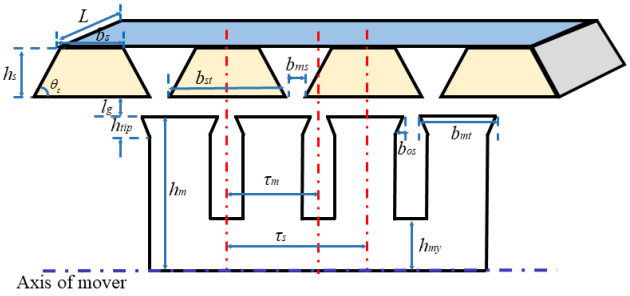

FIGURE 2. Specific dimensions of LSRMSS.

The NIF model is constructed and the dynamic performance of LSRMSS can be estimated by using the method of NIF [20].

The specific structure of this paper is organized as follows: Section II illustrates the specific structure of LSRMSS. In Section III, the LSRMSS using a nonlinear inductance model based on an equivalent magnetic circuit model is introduced. Besides, some key factors, including end effects and mutual inductance effects, are discussed. The experimental platform is set up, and then the experimental results are compared with the NIF results to verify the feasibility of NIF in Section IV. Relevant conclusions are drawn in Section V.

II. MACHINE STRUCTURE

The topology of LSRMSS presented in this paper is shown in Fig. 1. LSRMSS features a segmental stator and toroidal wound mover. The so-called segmental stator is composed of individual ferromagnetic segments, thus providing good potential to be used in long-distance propulsion systems. Besides, when the single-phase winding is energized, the flux of conventional LSRM only crosses through some parts of the stator yoke and leaves the other parts of the stator yoke free of flux. Therefore, the conventional LSRM has a lower utilization ratio of ferromagnetic material, resulting in a lower power and force density. For the presented LSRMSS, the flux goes through via the two adjacent mover teeth and stator segments. Thus, compared with conventional LSRM, it features a short magnetic circuit. In this case, the utilization ratio of ferromagnetic material has been significantly enhanced. In addition, there is only single-phase winding placed in each mover slot, which increases the slot-filling ratio of LSRMSS. Some measures of phase isolation that have been used in conventional LSRM are not required.

The specific dimensions of LSRMSS are listed in Table 1. The illustration of the geometric dimensions of LSRMSS is shown in Fig. 2.

III. MODELING OF LSRMSS USING ANALYTICAL APPROACH

A. NONLINEAR INDUCTANCE FUNCTION

This section aims to investigate the dynamic performance of LSRMSS using a nonlinear inductance model. Based on the EMC of LSRMSS at several special working positions, such as aligned positions and unaligned positions, the NIF model can be obtained [22], [23], [24], [25].

The equivalent magnetic circuit is established in Fig. 3. In this section, six EMCs at different positions are calculated. Among them, the schematic diagrams of magnetic flux paths and the EMC of the three main positions have been given in Fig. 3.

The specific EMC of LSRMSS with different positions is shown in Fig. 3. It can be seen that the flux paths can be divided into three parts: air gap, iron core, and slot, which can be calculated by different methods. This paper adopts a new method to reduce the calculation error. It can be seen from Fig. 4 that the first-layer cell is divided into four smaller

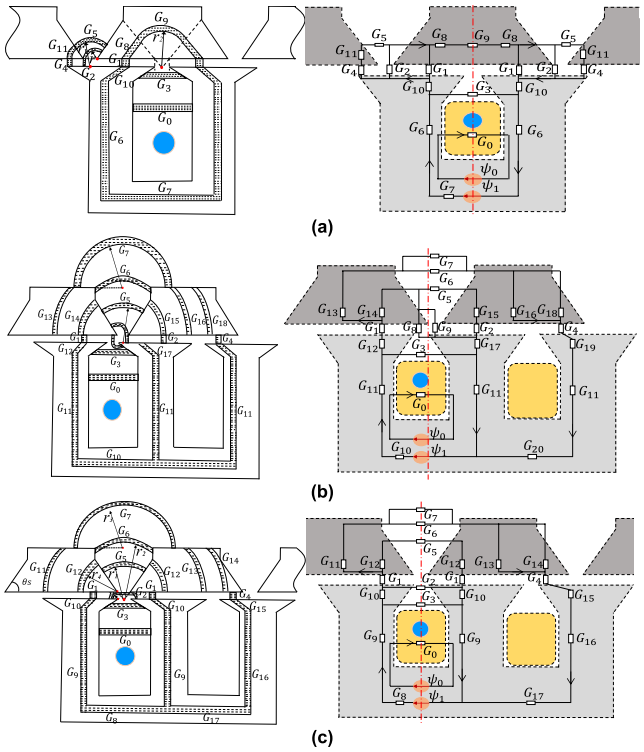

FIGURE 3. The magnetic circuit model of LSRM. (a) aligned position. (b) middle position. (c) unaligned position.

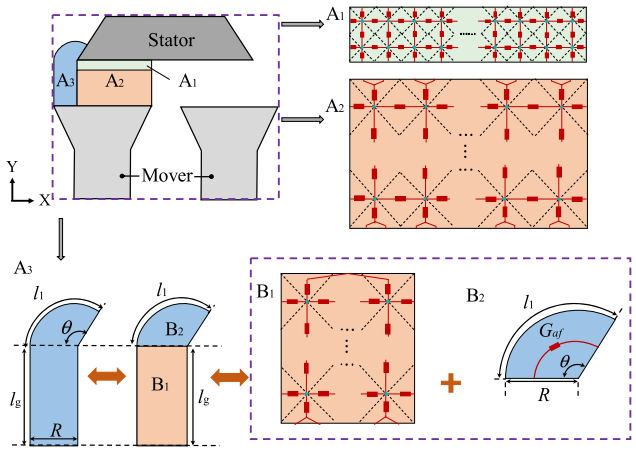

FIGURE 4. Mesh approach of air-gap.

cells. Thus, the changing process of flux magnetic reluctance is smoother.

The nonlinear region can be divided into four elements, i.e., stator yoke, stator tooth, mover yoke, and mover tooth. The magnetic motive force is located in the part of the mover yoke.

The iron core permeance changes along with the iron core permeability. In this paper, the iron core permeability is calculated by iterative approaches and the iron core permeability of each part is taken as an iterative variable. The flow chart of nonlinear analysis about iron core permeability is given in Fig. 5 and the calculation formulas are expressed

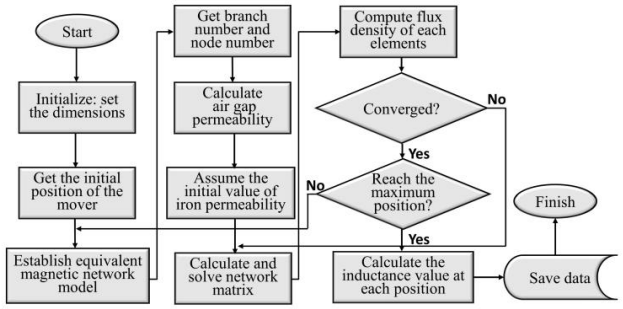

FIGURE 5. Flow chart of nonlinear analysis.

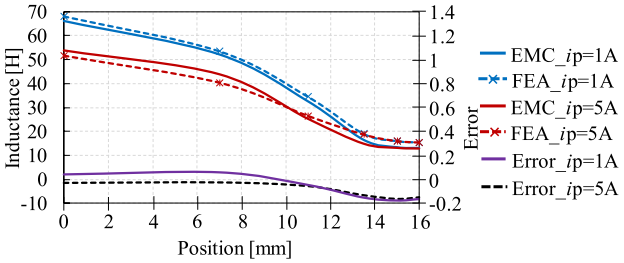

FIGURE 6. Comparison of EMC and FEA under different currents.

in equation (1) and equation (2). It can be seen from Fig. 5 that the result after n iterations will be used as the new initial value for the n+1th iteration step in this iterative process.

$$\lambda_i^{(k)} = \min\left\{1, 0.1 + \frac{C_d}{0.01 + (\mu(B_i^{(k+1)}) - \mu_i^{(k)})/\mu_i^{(k)}}\right\} \tag{1}$$

$$\mu_i^{(k+1)} = \mu_i^{(k)} + \lambda_i^{(k)}[\mu(B_i^{(k+1)}) - \mu_i^{(k)}] \tag{2}$$

where k is the number of iterations, $\lambda_i^{(k)}$ is the damping coefficient, and $\mu_i^{(k)}$ is the iron core permeability of the magnetic circuit after k iterations.

In order to verify the accuracy of the results calculated by the method of EMCs, the simulation model of LSRMSS has been established in the software of FEA. The inductance values at different locations calculated with MEC and FEA can be obtained as shown in Fig. 6.

The comparison results between the fitting curve and data points of inductance at currents of 1A and 5A are shown in Fig. 6. Besides, the error curves of inductance at currents of 1A and 5A are also shown in Fig. 6. It can be seen that the results of inductance at 1A using the method of EMC are more precise than at 5A. Meanwhile, the inductance error results of the aligned position are smaller than those of the unaligned position.

In order to obtain the inductance functions operating at different currents quickly and efficiently, a simple method is used in equation (3).

$$f_n(x) = (f(x) - L_{1\,\min})\left(\frac{L_{n\,\max} - L_{1\,\min}}{L_{1\,\max} - L_{1\,\min}}\right) + L_{1\,\min} \tag{3}$$

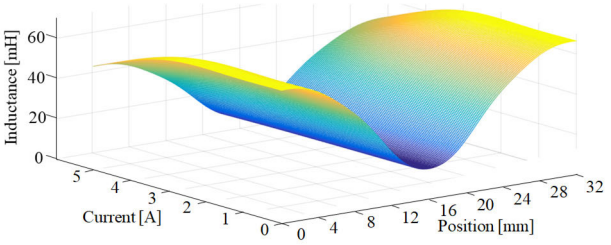

FIGURE 7. Fitting curves under different currents and different positions.

where $f_n(x)$ is the curve function at current of n A, $f(x)$ is the fitting function described at equation (4), $L_{n\,\max}$ is the maximum inductance at current of n A. $L_{1\,\min}$ and $L_{1\,\max}$ represent the minimum and maximum inductance at 1A, respectively.

In addition, the NIF in simulation model of LSRMSS f(x) can be expressed as equation (4):

$$f(x) = 0.0435 + 0.02679\cos(195.6x) - 0.003726\cos(391.2x) \tag{4}$$

The inductance values using the method of NIF under different currents and different positions can be obtained as shown in Fig. 7. Obviously, with the increasing of current, the peak of inductance waveform is declined and the minimum value always remains at the same level.

B. ESTABLISHING DYNAMIC MODEL

Most of the traditional research methods have low accuracy, which ignore the effect of magnetic saturation and use the linear model. This situation can be avoided by the NIF method using EMC-based inductance fitting curves.

The specific mathematical model of the LSRMSS based on NIF can be obtained and it has been expressed as equation (5).

$$\begin{cases} U_p = R_p i_p + \dfrac{d\psi_p}{dt} \\ \psi_A = L_p i_p \\ F_p = \dfrac{1}{2} i_p^2 \dfrac{dL_p}{vdt} \end{cases} \tag{5}$$

where U_p is the voltage of phase winding, R_p is the resistance, v is the speed of the motor, ψ_p is the flux linkage, L_p is the inductance.

The diagram of the LSRMSS system is shown in Fig. 8. The LSRMSS system can be divided into two parts: a drive circuit module and a correlation function calculation module. In the view of the correlation function calculation module, in order to obtain accurate calculation results, it is very important to establish a suitable inductance model.

The results considering magnetic saturation about currents, self-inductance, thrust, and back-EMF using different methods are shown in Fig. 9. The iron core will be saturated by increasing the armature current. The results based on the saturation of the iron core have been given above. In order to verify the feasibility and accuracy of the model building

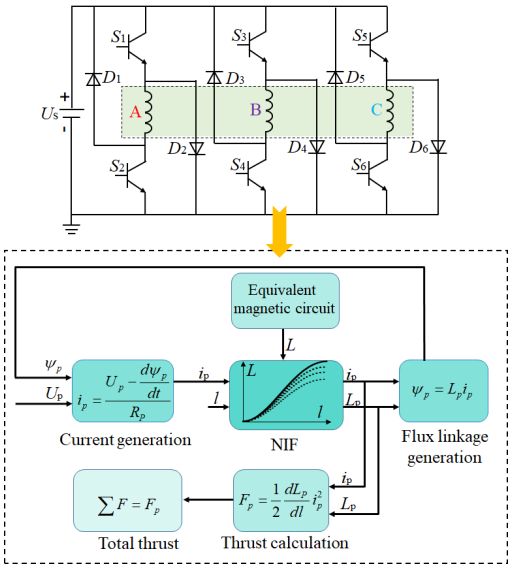

FIGURE 8. Diagram of the LSRMSS system.

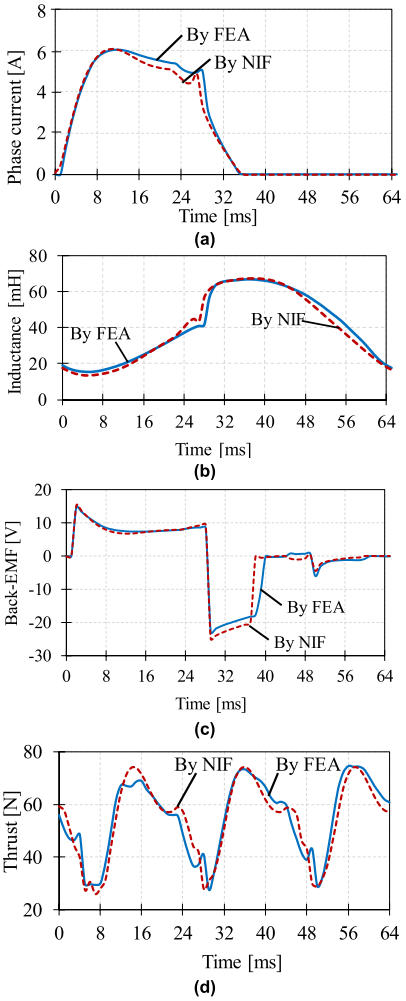

FIGURE 9. Comparison results between FEA and NIF at 0.5m/s considering iron core saturation. (a) Current. (b) Self-inductance. (c) Back-EMF. (d) Thrust.

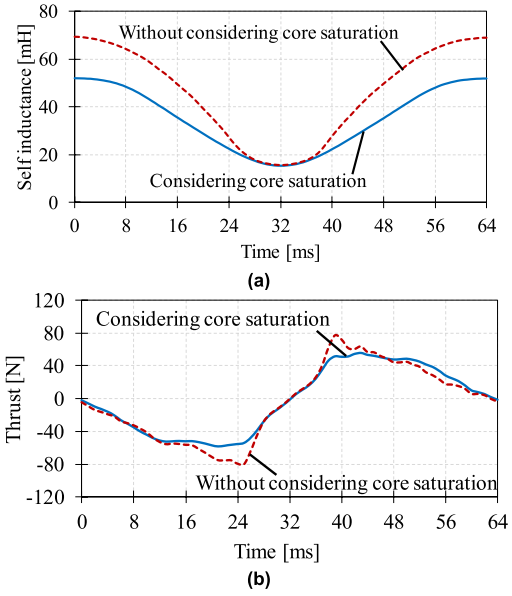

FIGURE 10. Comparison static results between considering core saturation and without considering core saturation at 5A and 0.5m/s. (a) Self-inductance. (b) Thrust.

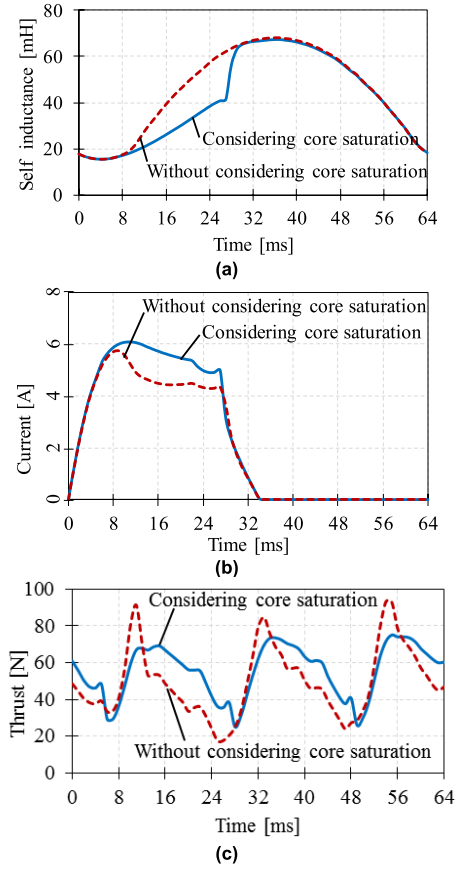

FIGURE 11. Comparison dynamic results between considering core saturation and without considering core saturation at 12V and 0.5m/s. (a) Self-inductance. (b) Current. (c) Thrust.

based on NIF, the specific results, including self-inductance, static thrust, dynamic current, and dynamic thrust, compared between considering core saturation and ignoring core saturation are shown in Figs. 10 and 11.

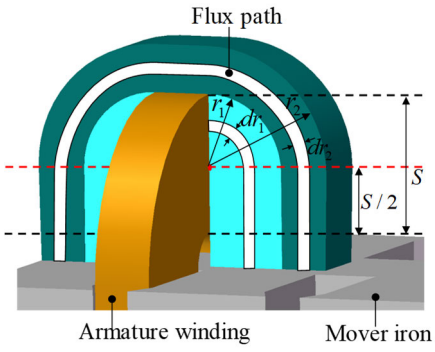

FIGURE 12. Distribution diagram of the ending effects about LSRMSS.

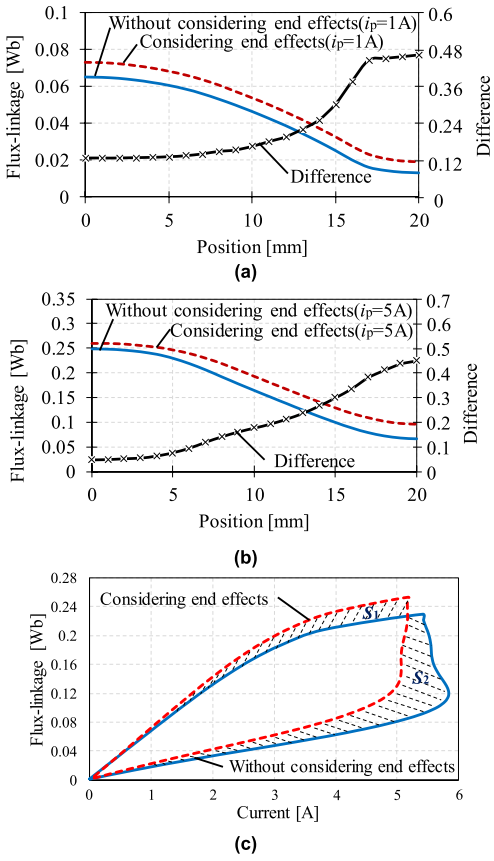

FIGURE 13. Flux linkage comparison results, (a) Flux linkage results Under 1A. (b) Flux linkage results Under 5A. (c) Flux linkage results Under different currents.

It can be seen from Fig. 9 that the results of NIF, including current, self-inductance, thrust, and back EMF, are all consistent with the waveforms of FEA. Thus, it is feasible for the system to use the method of NIF. In addition, the results using NIF have a subtle difference compared with the method of FEA due to the inductance results error between EMC and FEA.

C. END EFFECTS

End effects have always been a vital influencing factor in researching the performance of LSRMSS. The 2D FEA

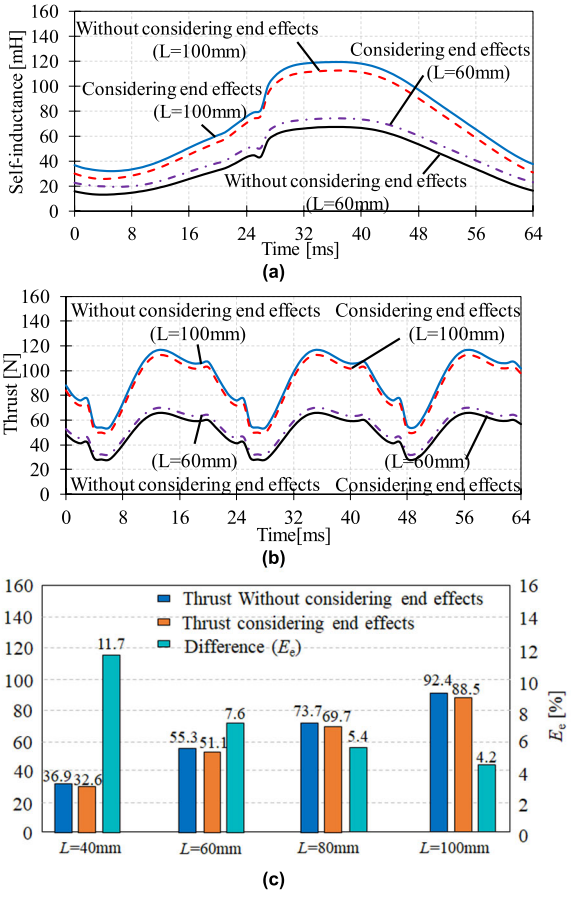

FIGURE 14. Comparison results at 60 or 100mm depth of stack length by NIF. (a) Self-inductance. (b) Thrust. (c) Average thrust.

simulation model can always be used to estimate and verify the rough dynamic performance characteristics. However, compared to the practical 3D FEA model, the errors of the 2D simulation model are obvious. Some of these errors are due to the end effects of armature windings, which can be clearly seen in Fig. 12.

It can be seen from Fig. 13 that the flux linkage values are different when considering end effects and without. Thus, it is significant to estimate the differences caused by end effects, which can improve the accuracy of the NIF method. Compared with conventional LSRM, special toroidal windings of LSRMSS determine that the end effects are low and invariable, which greatly cuts down the workload in NIF. The comparison results of flux linkage under different positions and currents are shown in Fig. 13. It can be seen from Fig. 13 (a) and (b) that the end effects on the aligned position are weaker than those on the unaligned position. In addition, it can be seen from Fig. 13 (c) that the energy of the magnetic field under end effects decreases obviously (S1<S2). Therefore, the horizontal thrust should theoretically be reduced due to end effects. The specific influence of end effects on self-inductance, thrust, and average thrust is shown in Fig. 14.

It can be seen from Fig. 14 that, due to the end effects of phase windings, the maximum value of self-inductance

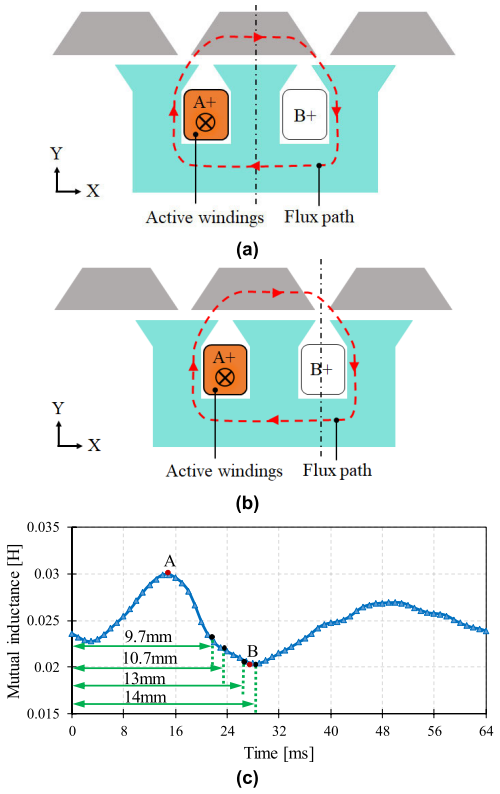

FIGURE 15. Schematic diagram of magnetic flux path and the waveform of mutual inductance. (a) The position with maximum mutual inductance. (b) The position with minimum mutual inductance. (c) The mutual inductance.

changes from 67.5 mH to 74.4 mH and the value of average thrust declines from 55.3 N to 51.1 N. The method of increasing the thickness of stacked silicon steel sheets is used to weaken the end effects or decrease the bad influence. Therefore, this paper also studies the laminated silicon steel sheet motor with a thickness of 100mm. The specific waveforms of self-inductance, thrust, and average thrust under 100mm stack length are also shown in Fig. 14.

It can be seen from Fig. 14 that with the increase in stack length, the values of current are invariable, and the self-inductance and thrust are changed proportionately. In order to obviously illustrate the effects of end windings, the expression of end effect percentage is defined, and the specific function is shown in equation (6).

$$E_e = \frac{F_{atw} - F_{ati}}{F_{atw}} \times 100\% \tag{6}$$

where F_{atw} is the average thrust when the motor is working without end effects, F_{ati} is the average thrust when it is working under influence of end effects. The specific comparison results are shown in Fig. 14 (c), which illustrate the end effects. Obviously, increasing stack length of LSRMSS can weaken the end effects. The value of E_e defined by equation (5) declines from 7.6% to 4.2% when the stack length is changed from 60mm to 100 mm.

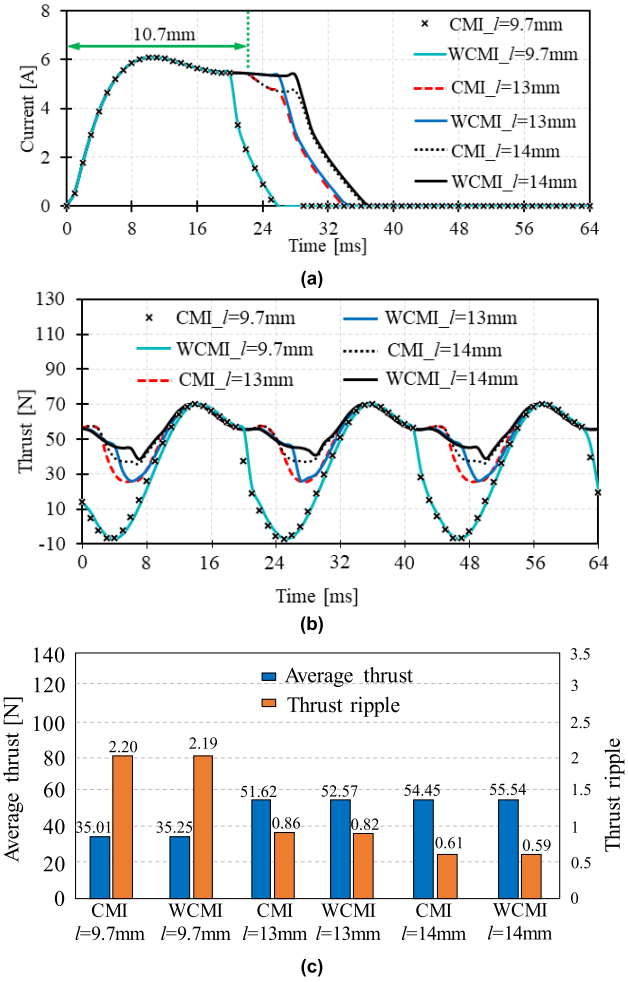

FIGURE 16. Effects of mutual inductance on dynamic performance of LRSMSS working at different excitation. (a) Phase currents. (b) Thrust. (c) Average thrust and thrust ripple.

D. MUTUAL INDUCTANCE

The influence of mutual inductance on dynamic performance is different when the motor is working in different states. When LSRMSS is working in a single-phase excitation state, the effects of mutual inductance are minimal. When LSRMSS is working in a double-phase excitation state, mutual inductance is a vital factor for LSRMSS to estimate dynamic performance. In this paper, the situation of double-phase excitation will appear when the operating period per phase is greater than 10.7mm. For LSRMSS, working in a double-phase excitation state can improve motor stability and weaken the force ripple. Thus, it is highly imperative to conduct research on mutual inductance.

To illustrate the influence of mutual inductance, the mutual inductance curves based on different excitation currents are researched. In addition, the maximum position is always invariable, and the special working position of the maximum point is shown in Fig. 15 (a). The position of minimum mutual inductance is shown in Fig. 15 (b).

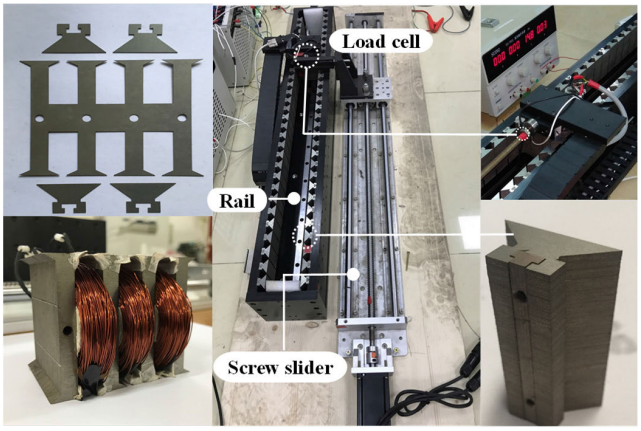

FIGURE 17. Prototype and experimental setup. (a) Lamination sheet and wound mover core. (b) Test platform. (c) Load cell and stator segment.

It can be seen from Fig. 15(a) that in the case of A-phase working solely, not only the magnetic flux goes through two adjacent mover teeth, but also a few of the magnetic flux is closed by B-phase winding. A schematic diagram of the minimum mutual inductance position is shown in Fig. 15(b). At this time, the interval between segmented secondary is aligned with the interval between mover. Meanwhile, the magnetic reluctance of the magnetic flux path about mutual inductance is the largest. This special characteristic of mutual inductance provides the basis for the research and optimization of LSRMSS.

In Fig. 16, "CMI" represents the results by considering mutual inductance effects, and "WCMI" represents the results without considering mutual inductance effects. It can be seen from Fig. 16 that the motor is working in different excitation states. In the case of $l = 9.7$ mm, the excitation period of each phase is less than 10.7 mm, and there is only one phase working at the same time.

Compared with the single-phase excitation state, the advantages of double-phase excitation ($l = 13$mm and $l = 14$mm) are obvious such as improvement of operating stability, decline of force ripple and increase of average thrust. Besides, the effects of mutual inductance cannot be ignored when LSRMSS is working at double-phase excitation state. It can be clearly seen from Fig. 16 (a) and (b) that the values of current and dynamic thrust are all decreasing due to the effects of mutual inductance. In conclusion, the effects of mutual inductance cannot be ignored when LSRMSS is working at double-phase excitation state.

IV. PROTOTYPE AND EXPERIMENT

The prototype is built according to the specific dimensions shown in Table 1. The prototype and experimental setup is shown in Fig. 17. A servo motor is used to drive the mover to be the required constant speed. The phase windings are controlled by the converter according to the real-time position feedback from the linear magnetic encoder. The phase current and thrust with different mover positions are measured by the current prove and force sensor, respectively.

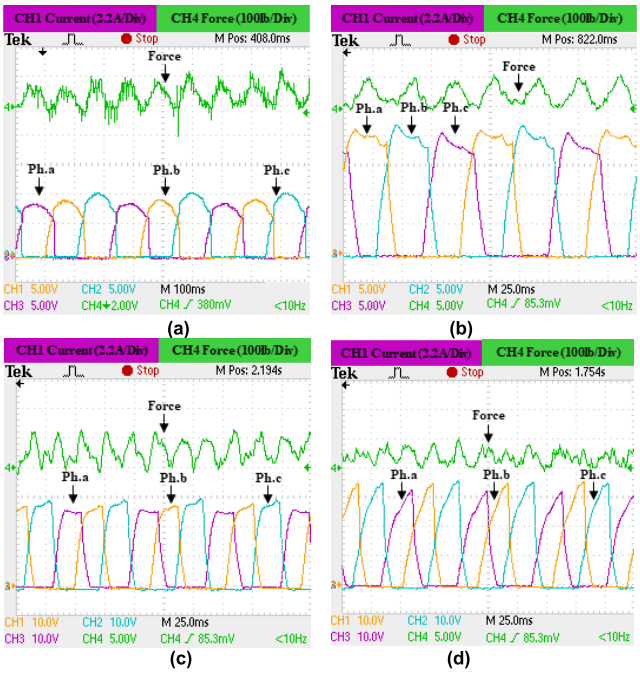

FIGURE 18. Measured phase current and force at different conditions. (a) Switch-on position is 13.8mm and switch-off position is 26mm at 7V, 0.1m/s. (b) Switch-on position is 13.8mm and switch-off position is 27mm at 16V, 0.4m/s. (c) Switch-on position is 13.8mm and switch-off position is 26mm at 24V, 0.5m/s. (d) Switch-on position is 13.8mm and switch-off position is 27mm at 24V, 0.5m/s.

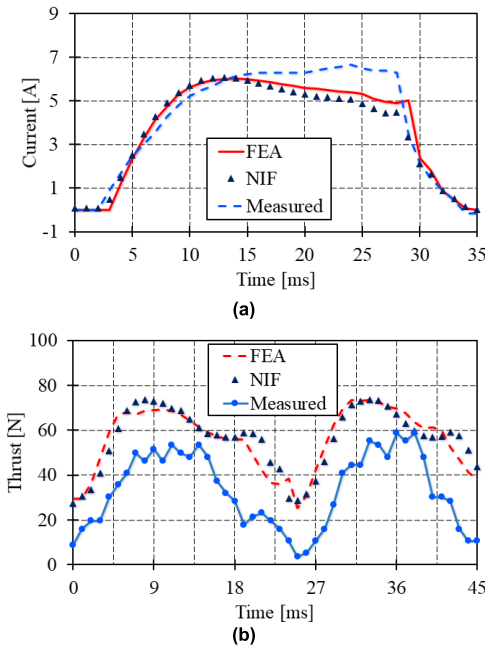

FIGURE 19. Comparison results between FEA, NIF simulation and measured at 24V and 0.5m/s. (a) Current. (b) Thrust.

The measured currents and thrust with different voltage supply, velocity and switched-on/off positions are shown in Fig. 18. The switch-on and switch-off positions refer to the positions at which the central line of mover slot align with the central line of stator segment. The results from FEA, NIF and practical measured results are compared.

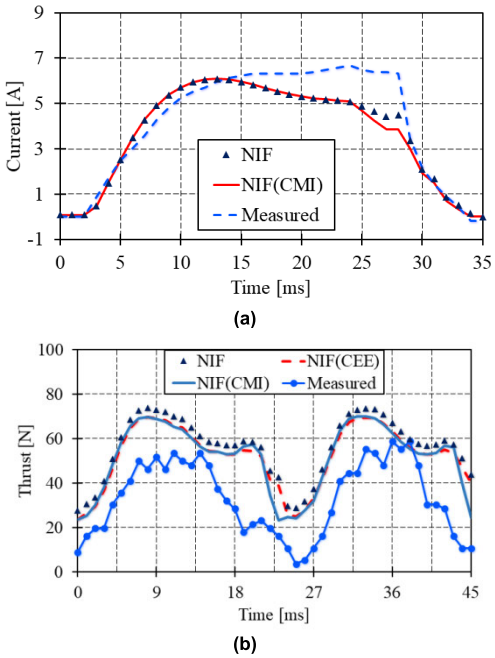

FIGURE 20. Comparison between NIF, improved NIF and measured results. (a) Current. (b) Thrust.

Fig. 19 shows the comparison results between FEA, NIF and measured results of phase current and thrust. The motor is supplied by the rated voltage 24V. The velocity of the motor is kept at the rated value 0.5m/s, and the phase winding is excited when the switch-on/off positions are 13.8mm/27 mm. The comparison of phase current is shown in Fig. 19 (a). It can be seen that the values of phase current obtained by the NIF model agree well with the FEA calculated results but has some errors compared to the measured results. Fig.19 (b) The measured thrust are compared by the NIF and FEA calculated results. Since the frictional force is not considered in the simulation, the measured thrust of the motor is smaller compared to the FEA and NIF calculated results.

Fig. 20 shows the comparison results between NIF, improved NIF and measured results of phase current and thrust. In Fig. 20, "CEE" represents the results by considering end effects. Through the above analysis, we should consider the influence of core saturation, end effects and mutual inductance on the results. As shown in Fig. 20 (a), the current obtained from NIF(CMI) drops faster than that from NIF at the initial stage after commutation, which is consistent with the change trend of measured result. As shown in Fig. 20 (b), the thrust considering end effects of phase windings is lower than that obtained from NIF without considering end effects. The thrust considering the mutual inductance is a little smaller than that without considering the mutual inductance.

In conclusion, the accuracy of the theoretical analysis, equivalent magnetic circuit model, and NIF model in this paper is verifies through the prototype fabrication, prototype test platform construction, and various prototype dynamic performance comparison test of LSRMSS, and the accuracy of the proposed NIF model in predicting the performance of the motor and the feasibility of the proposed NIF model in the control strategy are further verified.

V. CONCLUSION

An analytical nonlinear model of a linear switched reluctance motor with segmented secondary (LSRMSS) is developed to predict the dynamic performance of the machine. The nonlinear inductance function (NIF) is established considering the iron saturation effect, which is seen as the main feature of the linear reluctance machine, thus giving a high precision of performance prediction. The inductance values of LSRMSS with different positions through the reluctance equivalent network are obtained. Then the inductance functions under different currents and positions are fitted by the formula and compared with the FEA. Some key factors, such as the saturation of the iron core, the end effects and the mutual inductance, are considered. Compared to the FEA simulation, the presented nonlinear model is highly efficient for predicting machine performance. Finally, the prototype is fabricated, and the experiments are done. The feasibility of the model above is validated by comparing the analytically calculated results with the experimental results.

REFERENCES

[1] R. Cao, M. Cheng, C. Mi, W. Hua, and W. Zhao, "Comparison of complementary and modular linear flux-switching motors with different mover and stator pole pitch," *IEEE Trans. Magn.*, vol. 49, no. 4, pp. 1493–1504, Apr. 2013.

[2] R. Cao, M. Lu, N. Jiang, and M. Cheng, "Comparison between linear induction motor and linear flux-switching permanent-magnet motor for railway transportation," *IEEE Trans. Ind. Electron.*, vol. 66, no. 12, pp. 9394–9405, Dec. 2019.

[3] J.-Q. Li, W.-L. Li, G.-Q. Deng, and Z. Ming, "Continuous-behavior and discrete-time combined control for linear induction motor-based urban rail transit," *IEEE Trans. Magn.*, vol. 52, no. 7, pp. 1–4, Jul. 2016.

[4] Z. Han, J. Xu, W. Rui, and Y. Wang, "Effect of winding connections on thrust and current asymmetry of linear induction machines considering end effect," *IEEE Trans. Plasma Sci.*, vol. 48, no. 8, pp. 2816–2821, Aug. 2020.

[5] M. Galea, G. Buticchi, L. Empringham, L. de Lillo, and C. Gerada, "Design of a high-force-density tubular motor," *IEEE Trans. Ind. Appl.*, vol. 50, no. 4, pp. 2523–2532, Jul./Aug. 2014.

[6] H. Sun Lim, R. Krishnan, and N. S. Lobo, "Design and control of a linear propulsion system for an elevator using linear switched reluctance motor drives," *IEEE Trans. Ind. Electron.*, vol. 55, no. 2, pp. 534–542, Feb. 2008.

[7] N. S. Lobo, H. Sun Lim, and R. Krishnan, "Comparison of linear switched reluctance machines for vertical propulsion application: Analysis, design, and experimental correlation," *IEEE Trans. Ind. Appl.*, vol. 44, no. 4, pp. 1134–1142, Aug. 2008.

[8] S.-D. Huang, G.-Z. Cao, Z.-Y. He, C. Wu, J.-A. Duan, N. C. Cheung, and Q.-Q. Qian, "Maximum-force-per-ampere strategy of current distribution for efficiency improvement in planar switched reluctance motors," *IEEE Trans. Ind. Electron.*, vol. 63, no. 3, pp. 1665–1675, Mar. 2016.

[9] B. Zhang, J. Yuan, L. Qiu, N. Cheung, and J. F. Pan, "Distributed coordinated motion tracking of the linear switched reluctance machine-based group control system," *IEEE Trans. Ind. Electron.*, vol. 63, no. 3, pp. 1480–1489, Mar. 2016.

[10] G.-Z. Cao, N. Chen, S.-D. Huang, S.-S. Xiao, and J. He, "Nonlinear modeling of the flux linkage in 2-D plane for the planar switched reluctance motor," *IEEE Trans. Magn.*, vol. 54, no. 11, pp. 1–5, Nov. 2018.

[11] Y. Zou, K. E. Cheng, N. C. Cheung, and J. Pan, "Deformation and noise mitigation for the linear switched reluctance motor with skewed teeth structure," *IEEE Trans. Magn.*, vol. 50, no. 11, pp. 1–4, Nov. 2014.

[12] L. Qiu, Y. Shi, J. Pan, and G. Xu, "Networked H_∞ controller design for a direct-drive linear motion control system," *IEEE Trans. Ind. Electron*, vol. 63, no. 10, pp. 6281–6291, Oct. 2016.
[13] C.-T. Liu and T.-S. Chiang, "On the magnetic saturation analyses of a micro linear switched-reluctance motor," *IEEE Trans. Magn.*, vol. 40, no. 4, pp. 2861–2863, Jul. 2004.
[14] H. Chen, W. Yan, and Q. Wang, "Electromagnetic analysis of flux characteristics of double-sided switched reluctance linear machine," *IEEE Trans. Appl. Supercond.*, vol. 26, no. 4, pp. 1–7, Jun. 2016.
[15] W. Zhao, J. Zheng, J. Wang, G. Liu, J. Zhao, and Z. Fang, "Design and analysis of a linear permanent-magnet Vernier machine with improved force density," *IEEE Trans. Ind. Electron.*, vol. 63, no. 4, pp. 2072–2082, Apr. 2016.
[16] D. Wang, C. Peng, X. Yi, C. Huang, and X. Wang, "Multiple-phase excitation control of linear switched reluctance motor with segmented secondary driving system," in *Proc. 13th Int. Symp. Linear Drives Ind. Appl. (LDIA)*, Jul. 2021, pp. 1–6.
[17] G. Fang, J. Ye, D. Xiao, Z. Xia, and A. Emadi, "Computational-efficient model predictive torque control for switched reluctance machines with linear-model-based equivalent transformations," *IEEE Trans. Ind. Electron.*, vol. 69, no. 6, pp. 5465–5477, Jun. 2022.
[18] L. Ge, J. Zhong, C. Bao, S. Song, and R. W. De Doncker, "Continuous rotor position estimation for SRM based on transformed unsaturated inductance characteristic," *IEEE Trans. Power Electron.*, vol. 37, no. 1, pp. 37–41, Jan. 2022.
[19] S.-M. Jang, J.-H. Park, J.-Y. Choi, and H.-W. Cho, "Analytical prediction and measurements for inductance profile of linear switched reluctance motor," *IEEE Trans. Magn.*, vol. 42, no. 10, pp. 3428–3430, Oct. 2006.
[20] J. F. Pan, N. C. Cheung, and Y. Zou, "An improved force distribution function for linear switched reluctance motor on force ripple minimization with nonlinear inductance modeling," *IEEE Trans. Magn.*, vol. 48, no. 11, pp. 3064–3067, Nov. 2012.
[21] G. Liu, S. Jiang, W. Zhao, and Q. Chen, "Modular reluctance network simulation of a linear permanent-magnet Vernier machine using new mesh generation methods," *IEEE Trans. Ind. Electron.*, vol. 64, no. 7, pp. 5323–5332, Jul. 2017.
[22] J. G. Amoros and G. P. Andrada, "Magnetic circuit analysis of a linear switched reluctance motor," in *Proc. 13th Eur. Conf. Power Electron. Appl.*, Barcelona, Spain, Sep. 2009, pp. 1–9.
[23] Y. Liu, H. Yu, and Y. Wang, "Establishment of a new dual rotor flux switching motor magnetic circuit model and optimization of no-load back EMF," *IEEE Trans. Magn.*, vol. 55, no. 12, pp. 1–5, Dec. 2019.
[24] Y. Laoubi, M. Dhifli, G. Verez, Y. Amara, and G. Barakat, "Open circuit performance analysis of a permanent magnet linear machine using a new hybrid analytical model," *IEEE Trans. Magn.*, vol. 51, no. 3, pp. 1–4, Mar. 2015.
[25] Y. Huang, T. Zhou, J. Dong, H. Lin, H. Yang, and M. Cheng, "Magnetic equivalent circuit modeling of yokeless axial flux permanent magnet machine with segmented armature," *IEEE Trans. Magn.*, vol. 50, no. 11, pp. 1–4, Nov. 2014.

ZHIPENG LI received the B.S. degree in electrical engineering from Qingdao Agricultural University, Jinan, China, in 2022. He is currently pursuing the M.S. degree in electrical engineering with the School of Electrical Engineering, Shandong University, Jinan.

His research interests include application-oriented electrical drives and intelligent control.

DAOHAN WANG (Member, IEEE) received the B.Eng., M.Eng., and Ph.D. degrees in electrical engineering from Shandong University, in 2003, 2006, and 2010, respectively.

From 2011 to 2012, he was a Postdoctoral Researcher with Dong-A University, Busan, South Korea, where his work was supported by Research Foundation for Industrial-Academy Cooperation, South Korea. From 2012 to 2013, he was a Research Fellow with Sungkyunkwan University, Suwon, South Korea. Since 2013, he has been with Shandong University, where he is currently a Professor with the School of Electrical Engineering. His research interests include application-oriented electrical drives and intelligent control, energy-saving techniques, and sustainable energy conversion.

CAN HUANG received the B.S. degree in electrical engineering from Shandong University, Jinan, China, in 2019, and the M.S. degree in electrical engineering from the School of Electrical Engineering, Shandong University, in 2023.

He is currently with Shandong Electric Power Engineering Consulting Institute Company Ltd. His research interests include application-oriented electrical drives and intelligent control.

SHUANG XU received the B.S. degree in electrical engineering from Dalian Maritime University, Dalian, China, in 2021. He is currently pursuing the M.S. degree in electrical engineering with the School of Electrical Engineering, Shandong University, Jinan, China.

His research interests include application-oriented electrical drives and intelligent control.

XIUHE WANG (Member, IEEE) was born in China, in July 1967. He received the B.E. and M.E. degrees in electrical engineering from Shandong University, in 1989 and 1993, respectively, and the Ph.D. degree in electrical engineering from the Shenyang University of Technology, in 1996.

From 2001 to 2002, he was a Postdoctoral Fellow with Seoul National University, Seoul, South Korea. He is currently a Professor in electrical engineering and the Vice Head of the School of Electrical Engineering, Shandong University, China. His research interests include permanent magnet machines, energy-efficient machines, theoretical analysis, and the calculation of electromagnetic devices, and its application on electrical machines. He has published more than 100 papers on these topics.